

## Effect of Quantum Barrier Thickness on the Optical Properties of Triple Triangular GaAs/AlGaAs Quantum Wells

Behçet Özgür Alaydın<sup>1,a,\*</sup>

<sup>1</sup> Department of Electronics and Automation, Sivas Cumhuriyet University, 58140, Sivas, Türkiye

\*Corresponding author

### Research Article

#### History

Received: 23/09/2024

Accepted: 29/12/2024



This article is licensed under a Creative Commons Attribution-NonCommercial 4.0 International License (CC BY-NC 4.0)

### ABSTRACT

This study investigates the electronic and optical properties of a GaAs/Al<sub>x</sub>Ga<sub>1-x</sub>As triple triangular quantum well (QW) structure, focusing on the 2 – 4 and 3 – 4 intersubband transitions. By varying the right barrier (R<sub>b</sub>) thickness from 0 to 6 nm, the impact on wave function localization, energy levels, dipole moment matrix elements, absorption coefficients, and refractive index changes was analyzed using a finite element-based Schrödinger solver. Quantitative results indicate that increasing the R<sub>b</sub> breaks the symmetry of the potential, enabling the 2 – 4 transition and causing variations in absorption coefficients, which peak at 4 nm before declining. The 3 – 4 transition exhibits a higher and more stable total absorption coefficient compared to the 2 – 4 transition, ranging from 1100 to 1125 cm<sup>-1</sup>. Additionally, the total refractive index changes for the 3 – 4 transition remain constant (±0.006 to ±0.009), while the 2 – 4 transition shows more variation (±0.001). Qualitatively, the 3 – 4 transition's stability and minimal energy difference from the 2 – 4 transition make it a more promising candidate for terahertz device applications, particularly where R<sub>b</sub> thickness constraints are present. These findings underscore the importance of barrier engineering in optimizing QW-based devices for advanced semiconductor application.

**Keywords:** GaAs, AlGaAs, Quantum Well, Absorption Coefficients, Refractive Index Change.

<sup>a</sup> [balaydin@cumhuriyet.edu.tr](mailto:balaydin@cumhuriyet.edu.tr)

<https://orcid.org/0000-0003-0935-4836>

## Introduction

Advances in semiconductor (SC) device technology have increasingly impacted daily life, even though many SC devices have reached a point of efficiency saturation. However, improvements in artificial intelligence (AI) have introduced new perspectives on SC devices due to the microchips used as essential hardware for AI. As a result, research on SC devices has accelerated in recent years.

Researchers are striving to develop more efficient SC devices, with many focusing on fundamental aspects such as nanoscale quantum wells (QWs). State-of-the-art devices and record-breaking performances continue to be achieved with QW-based devices, and enhancing QW efficiency is widely believed to be key to further improvements. For this reason, I have studied the triple triangular QW structure to investigate the electronic and optical properties of the GaAs/Al<sub>x</sub>Ga<sub>1-x</sub>As QWs structure.

In literature, numerous studies have been published, many of which are still under review. Öztürk et al. [1] examined the dependence of intersubband transitions in QWs on intense laser fields (ILF). Sayrac et al. [2] investigated the modulation of harmonic generation coefficients (HGC) in n-type quadruple  $\delta$ -doped GaAs QWs under external fields. Restrepo et al. [3] studied mid-infrared linear optical transitions in  $\delta$ -doped AlGaAs/GaAs triple QWs. Martinez-Orozco et al. [4] focused on nonlinear optical absorption (OA) and refractive index change (RIC) for field-effect transistor under hydrostatic pressure. Ozturk et al. [5] explored the effect of ILFs on

the nonlinear optical properties of triple QWs with parabolic and inverse-parabolic profiles. Alaydin [6] analyzed the optical properties of GaAs/Al<sub>x</sub>Ga<sub>1-x</sub>As superlattices under an electric field. Dakhlaoui published results on linear and nonlinear OA coefficients and RICs in GaN/Al<sub>x</sub>Ga<sub>1-x</sub>N double QWs operating at 1.55  $\mu$ m [7]. Durmuslar [8] investigated the nonlinear optical properties of double V-shaped Al<sub>x</sub>Ga<sub>1-x</sub>As/GaAs QWs, for structural parameters under ILF. Magdaleno et al. [9] examined asymmetric GaAs n-type double  $\delta$ -doped QWs, focusing on the effects of an applied electric field. Barseghyan et al. [10] studied the donor binding energy and photoionization cross sections in a Pöschl–Teller QW. Karabulut et al. [11] investigated linear and nonlinear intersubband OAs in asymmetric rectangular QWs. Sayrac [12] explored the nonlinear optical properties of semi-exponential QWs. Karimi et al. [13] analyzed linear and nonlinear intersubband OA and RICs in QWs. Niculescu et al. [14] studied the density of impurity states of shallow donors in a QW under ILF. Liu et al. [15] detailed electric field effects on HGC in Al<sub>x</sub>Ga<sub>1-x</sub>As/GaAs QWs. Altun et al. [16] analyzed the linear and nonlinear optical properties of a superlattice with periodically increased well width under electric and magnetic fields. All these studies have contributed to advancements in QW technology.

In this study, I investigated the absorption coefficients and refractive index changes of the (2-4) and (3-4) transitions of triple triangular QWs. The quantum barrier

(QB) thickness on the right side varies from 0 to 6 nm in 1 nm increments. The paper is organized into three sections: i) Section II provides the theoretical background of the triple triangular QW structure; ii) Section III discusses the computational results; iii) Section IV concludes the paper.

## Theory

A time-independent, one-dimensional Schrödinger equation is solved using a custom in-home Matlab code based on the finite element method [16, 17]. During the calculation, all operators are first created, and then the Hamiltonian is constructed. Diagonalization is subsequently performed to compute the eigenfunctions. In the end, the wave functions (WFs) and corresponding energy levels (ELs) are obtained under the effective mass approximation. The Hamiltonian for the triangular GaAs/Al<sub>x</sub>Ga<sub>1-x</sub>As QWs structure, featuring a periodically increasing right barrier, is provided in Equation (1).

$$H = -\frac{\hbar^2}{2m^*} \frac{d^2}{dz^2} + V(z) \quad (1)$$

where the second-order differential is written as:

$$\frac{d^2}{dz^2} = [-2 \text{diag}(\text{ones}(1, N_z)) + \text{diag}(\text{ones}(1, N_z - 1), -1) + \text{diag}(\text{ones}(1, N_z - 1), 1)]^2 \quad (2)$$

Here,  $m^*$  represents the effective mass of the electron, taken as 0.067  $m_0$  due to the lattice matching between GaAs and Al<sub>x</sub>Ga<sub>1-x</sub>As ( $m_0$  being the free electron mass).  $e$  is the electron charge,  $N_z$  defines the matrix length of the total quantum region. The length of  $N_z$  determines the size of the diagonalization matrix. A resolution step size of 1 Å is used, which results in a diagonalization matrix size of 600, and  $V(z)$  represents the confinement potential. The QW structure consists of three triangular QWs, each with a width of 12 nm. The quantum barrier (QB) between the left and middle QWs is 0, while the QB between the middle and right QWs increases from 0 to 6 nm in 1 nm increments. For the GaAs/Al<sub>x</sub>Ga<sub>1-x</sub>As QW structure, the conduction band offset and potential discontinuity  $V_0$  are set to 0.6 and 228 meV (corresponding to Aluminium concentration of 0.3), respectively [18, 19].

To solve the time-independent Schrödinger equation, diagonalization is performed in one dimension. After obtaining the ELs and their corresponding WFs, the linear absorption coefficients (LACs), third order nonlinear absorption coefficients (NACs), and total absorption coefficients (TACs) for the (2 – 4) and (3 – 4) intersubband transitions are calculated for the first four ELs using the density matrix approach [20, 21].

$$\beta_{if}^{(1)}(\omega) = \omega \sqrt{\frac{\mu}{\epsilon_r}} |M_{if}|^2 \frac{e^2 \sigma_v \hbar \Gamma}{(E_{if} - \hbar\omega)^2 + (\hbar \Gamma)^2} \quad (3)$$

$$\beta_{if}^{(3)}(\omega, I) = -2\omega \sqrt{\frac{\mu}{\epsilon_r}} |M_{if}|^4 \left( \frac{I}{\epsilon_0 c n_r} \right) \frac{e^4 \sigma_v \hbar \Gamma}{\{(E_{if} - \hbar\omega)^2 + (\hbar \Gamma)^2\}^2} \times \left[ 1 - \frac{|\delta_{if}|^2}{|2M_{if}|^2} \left( \frac{(E_{if} - \hbar\omega)^2 - (\hbar \Gamma)^2 + 2E_{if}(E_{if} - \hbar\omega)}{(E_{if})^2 + (\hbar \Gamma)^2} \right) \right] \quad (4)$$

$$\beta_{if}(\omega, I) = \beta_{if}^{(1)}(\omega) + \beta_{if}^{(3)}(\omega, I) \quad (5)$$

The linear refractive index change (LRICs), non-linear refractive index change (NRICs), and total refractive index change (TRICs) can be formulated as follows [22, 23]:

$$\frac{\Delta n_{if}^{(1)}(\omega)}{n_r} = \frac{e^2 \sigma_v}{2\epsilon_0 n_r^2} |M_{if}|^2 \frac{(E_{if} - \hbar\omega)}{(E_{if} - \hbar\omega)^2 + (\hbar \Gamma)^2} \quad (6)$$

$$\frac{\Delta n_{if}^{(3)}(\omega, I)}{n_r} = -\frac{\mu c}{4 \epsilon_0 n_r^3} |M_{if}|^2 \frac{e^4 \sigma_v I}{\{(E_{if} - \hbar\omega)^2 + (\hbar \Gamma)^2\}^2} \times \left[ 4(E_{if} - \hbar\omega) |M_{if}|^2 - \frac{\delta_{if}^2}{(E_{if})^2 + (\hbar \Gamma)^2} \times \{(E_{if} - \hbar\omega)[E_{if}(E_{if} - \hbar\omega) - (\hbar \Gamma)^2] - (\hbar \Gamma)^2 [2E_{if} - \hbar\omega]\} \right] \quad (7)$$

$$\frac{\Delta n_{if}(\omega, I)}{n_r} = \frac{\Delta n_{if}^{(1)}(\omega)}{n_r} + \frac{\Delta n_{if}^{(3)}(\omega, I)}{n_r} \quad (8)$$

Intersubband dipole moment matrix elements (DMMEs) are obtained by

$$M_{if} = \int \Psi_f^* z \Psi_i dz, \quad (i, f = 1, 2, 3, 4) \quad (9)$$

Here,  $\delta_{if} = M_{ff} - M_{ii}$  represents the intra-subband DMMEs,  $I$  is the optical light intensity, and  $\omega$  is the angular frequency of the incident photon.  $E_{if} = E_f - E_i = \hbar \omega_{if}$ , where  $E_f$  and  $E_i$  represent the quantized ELs of the final and initial states, respectively.  $\epsilon_0$  is the vacuum permittivity,  $\epsilon_r$  is the real part of the permittivity,  $\mu$  is the magnetic permeability,  $n_r$  is the refractive index, and  $\sigma_v$  is the carrier density.

## Result and Discussion

I have theoretically studied the electronic and optical properties for the (2 – 4) and (3 – 4) transitions in the triple triangular QW structure. Other transitions, such as (1 – 2), (1 – 3), (1 – 4) and (2 – 3), were not included in the study due to negligibly small values (the DMME, TAC and RIC values are lower than  $10^{-24}$ ). In this study, I have used  $\sigma_v = 4 \times 10^{16} \text{ cm}^{-3}$ ,  $T = 1 / \Gamma = 0.14 \text{ ps}$  and an optical intensity  $I = 0.5 \text{ MW/cm}^2$  [24, 25].

Figure 1 shows the potential variation of the triple triangular QWs for different right barrier ( $R_B$ ) widths. When the  $R_B$  is 0 nm, the ground state EL (blue line) is distributed across the wells, with most localization in the middle QW. A similar behavior is observed for the second excited state (green line). The first excited state (red line), however, localizes in the left and right barriers, while the third excited state (pink line) shows an irregular distribution across the QW region. As the  $R_B$  increases from 0 to 2 nm, the symmetry of the potential is broken,

leading to changes in the localization of the states. The ground and second excited states shift to the left and middle QWs, with their probability in the right well dropping to almost zero. In contrast, the first excited state becomes localized in the right QW. The irregular distribution of the third excited state remains but starts to shift toward the left side of the QW region. These changes are attributed to the broken symmetry. With further increases in  $R_B$  thickness (4 nm and 6 nm), the localization

of states becomes more defined. The ground and second excited states are primarily confined to the left and middle QWs, with no localization in the right QW. The first excited state is fully localized in the right well, while the third excited state shows significant distribution in the left and middle QWs. It is evident that  $R_B$  thickness disrupts the symmetry in the structure, although some coupling between the wells remains.

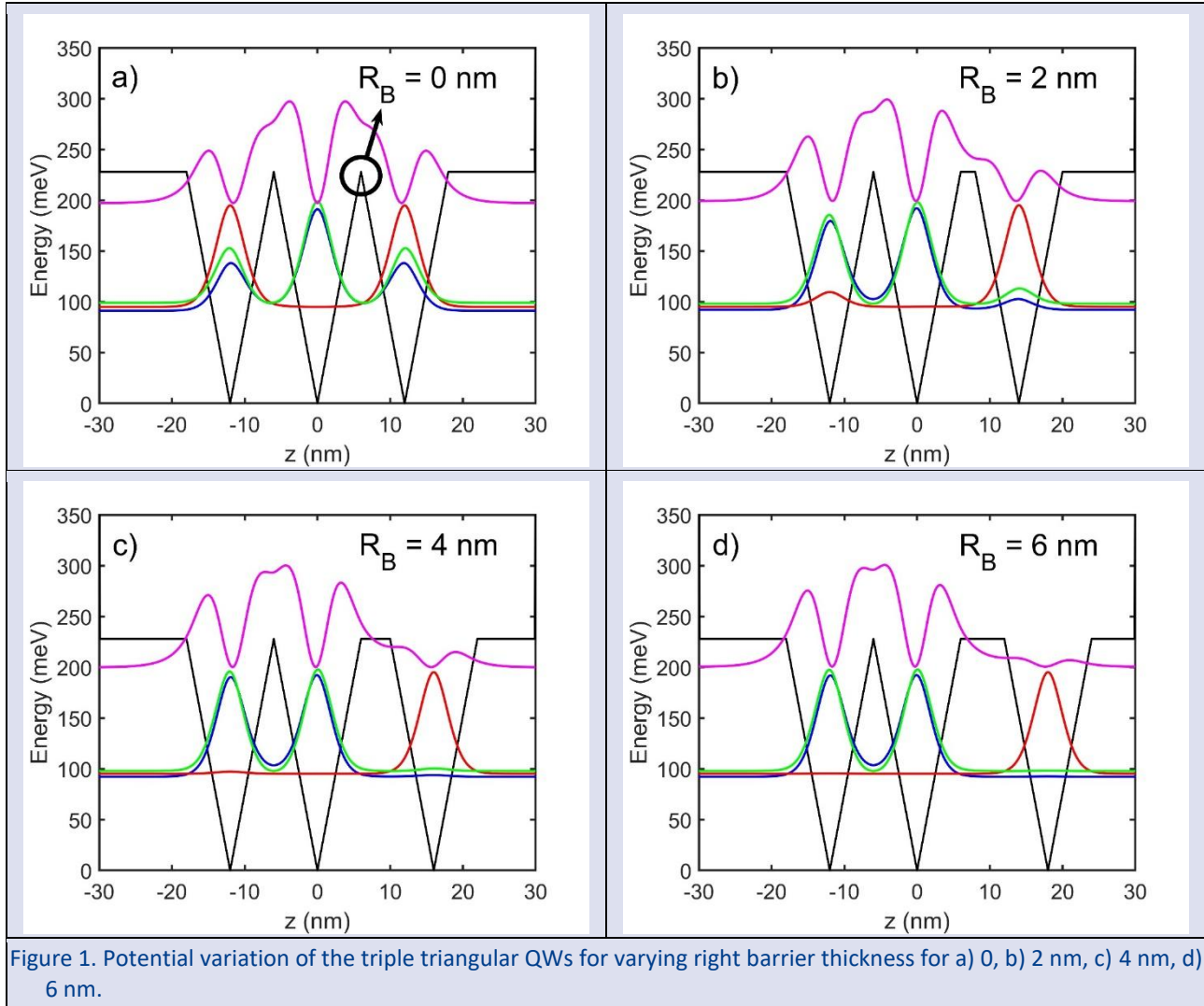


Figure 1. Potential variation of the triple triangular QWs for varying right barrier thickness for a) 0, b) 2 nm, c) 4 nm, d) 6 nm.

Figure 2 illustrates the variation of ELs, energy differences, and DMMEs as a function of the right barrier  $R_B$ . As shown in Figure 2a, the ELs are minimally affected by changes in  $R_B$  thickness. Consequently, the energy differences for the 2 – 4 and 3 – 4 transitions vary within a small range, with approximate differences of 3 meV and 5 meV, respectively. In Figure 2b, the DMMEs for the 2 – 4 and 3 – 4 transitions, along with the intersubband transitions for the 2 – 4 and 3 – 4 levels, are presented. The DMMEs for the 1 – 2, 1 – 3, 1 – 4 and, 2 – 3 transitions are zero and are not shown. While it is

understood that the 3 – 4 transition is more probable and more than an order of magnitude higher than the 2 – 4 transition, both transitions are largely independent of the  $R_B$  thickness. The intersubband DMMEs ( $\delta_{34}, \delta_{24}$ ) for these transitions are proportional to the  $R_B$  thickness, with the rate of increase for the 3 – 4 transition consistently higher than that of the 2 – 4 transition. This further supports the conclusion that the 3 – 4 transition is more probable than the 2 – 4 transition.

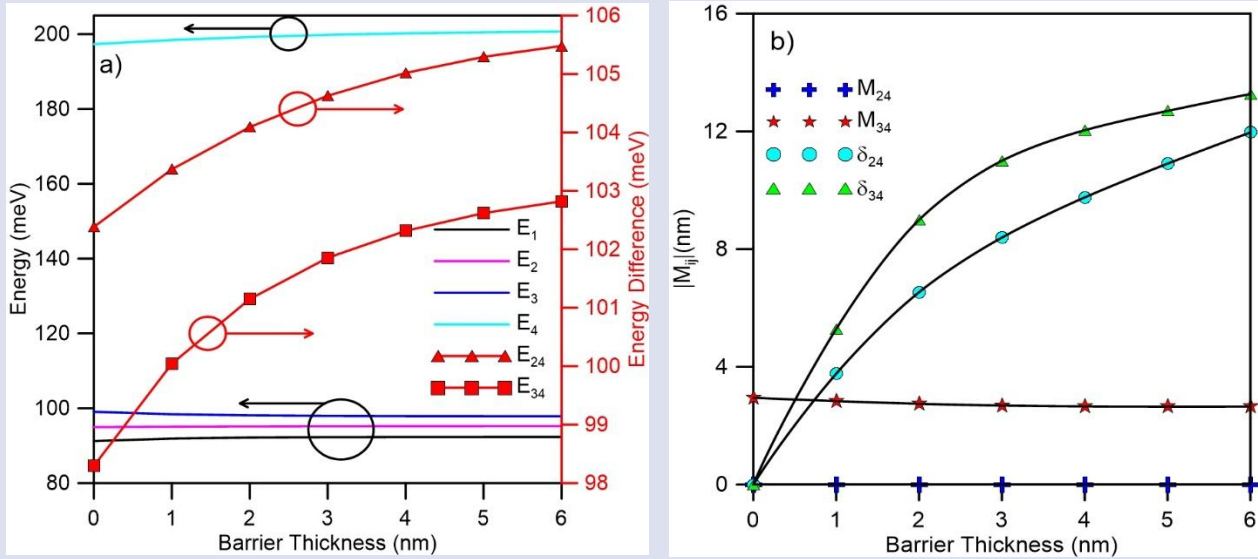


Figure 2. a) Variation of the ELs and energy differences, b) variation of the DMMEs.

In Figure 3, LACs, NACs, and TACs of the 2 – 4 transition are presented. When the  $R_B$  is zero, the absorption coefficients are also zero due to the symmetry of the structure. As the  $R_B$  increases, LAC, NAC, and TAC become non-zero due to the broken symmetry and the shift in the WFs, which alters the DMME and enables the 2 – 4 transition. With 1 nm increments in  $R_B$  thickness, LAC, NAC, and TAC increase up to 4 nm, after which further increases in  $R_B$  thickness result in a noticeable decrease in the absorption coefficients. The TAC reaches approximately  $69 \text{ cm}^{-1}$  due to  $\delta_{24}$  which is increasing. The absorption coefficients for the 2 – 4 transition are comparable to values reported in the literature [3, 8, 19]. Additionally, a slight blue shift is observed in the optical

spectrum, resulting from the small increase in energy difference, as mentioned earlier.

In Figure 4, LACs, NACs, and TACs of the 3 – 4 transition are plotted. For an  $R_B$  of 0 nm, the LAC is approximately  $2086 \text{ cm}^{-1}$ . However, as the  $R_B$  increases, the LAC decreases almost linearly, down to around  $1760 \text{ cm}^{-1}$ . This decline is due to the reduction of  $M_{34}$ , as shown in Figure 2b. Despite the changes in LAC, the TAC for the 3 – 4 transition remains largely unaffected by  $R_B$  variation. This is because the NAC decreases in inverse proportion to the linear reduction in LAC, owing to the more significant increase in  $\delta_{34}$  compared to  $M_{34}$ . As a result, the TAC fluctuates between approximately 1100 and  $1125 \text{ cm}^{-1}$ . Similar to the 2 – 4 transition, a slight blue shift is also observed in the 3 – 4 transition.

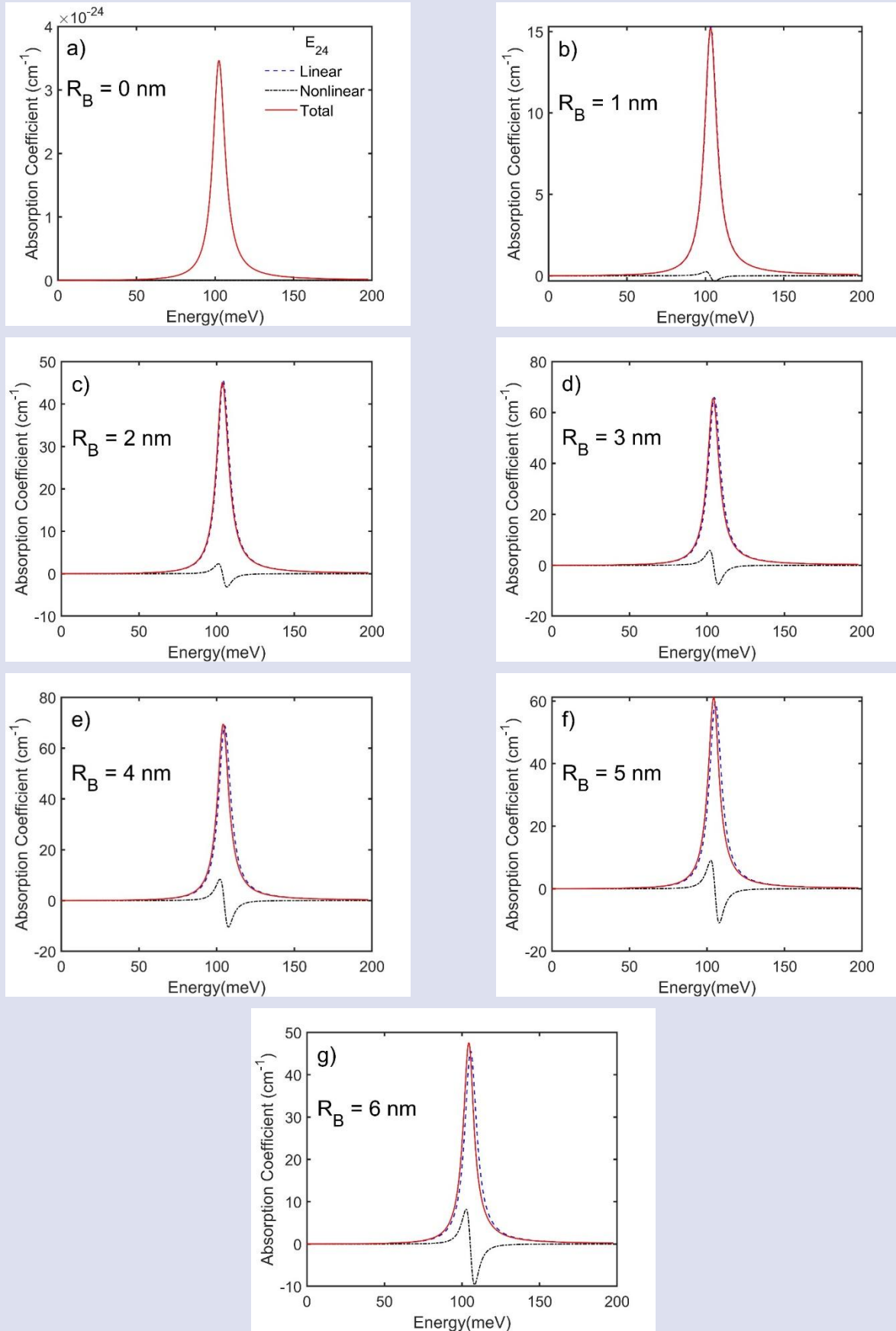


Figure 3. LACs, NACs and TACs of the 2 – 4 transition for varying  $R_B$  thickness.

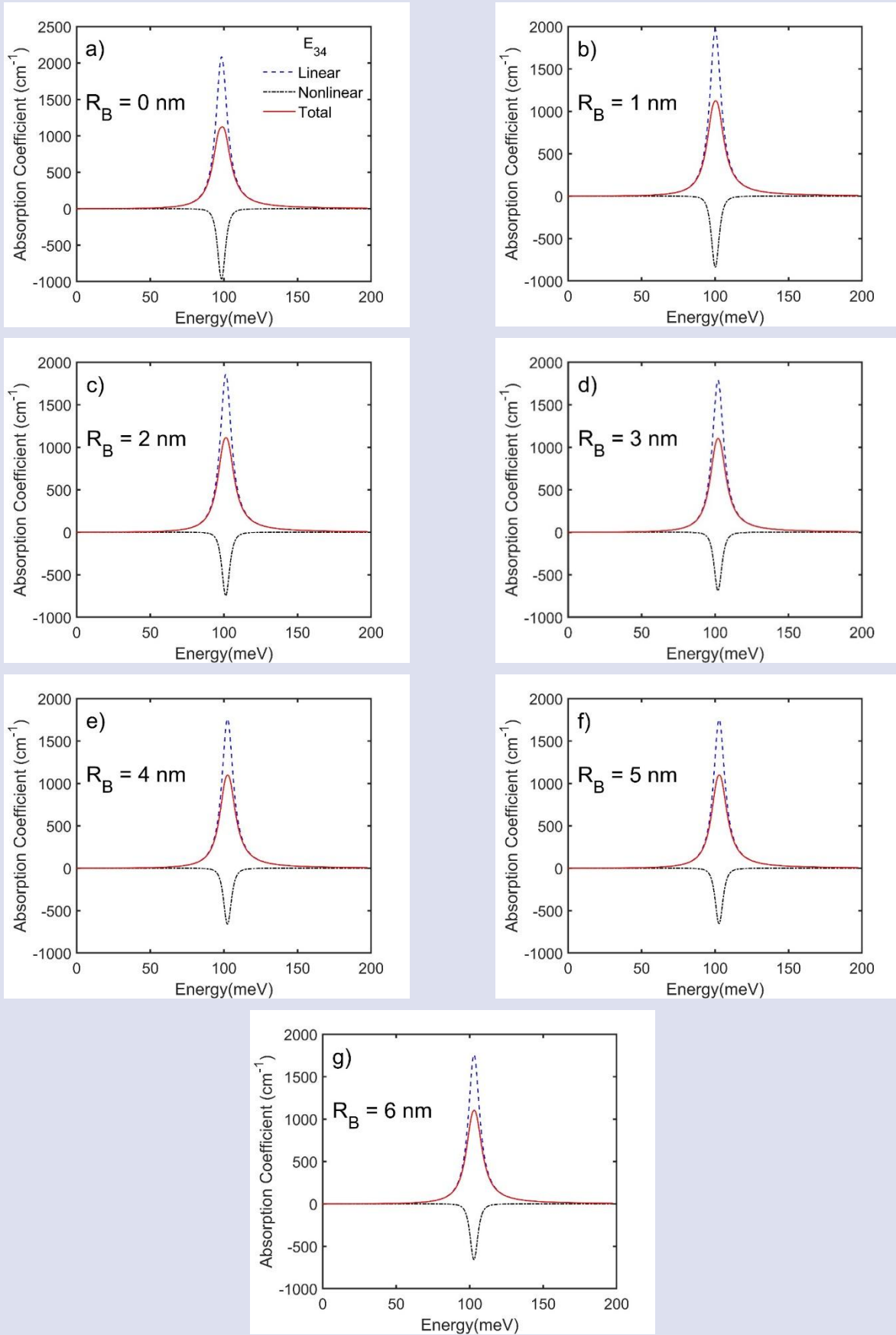


Figure 4. LACs, NACs and TACs of the 3 – 4 transition for varying  $R_B$  thickness.

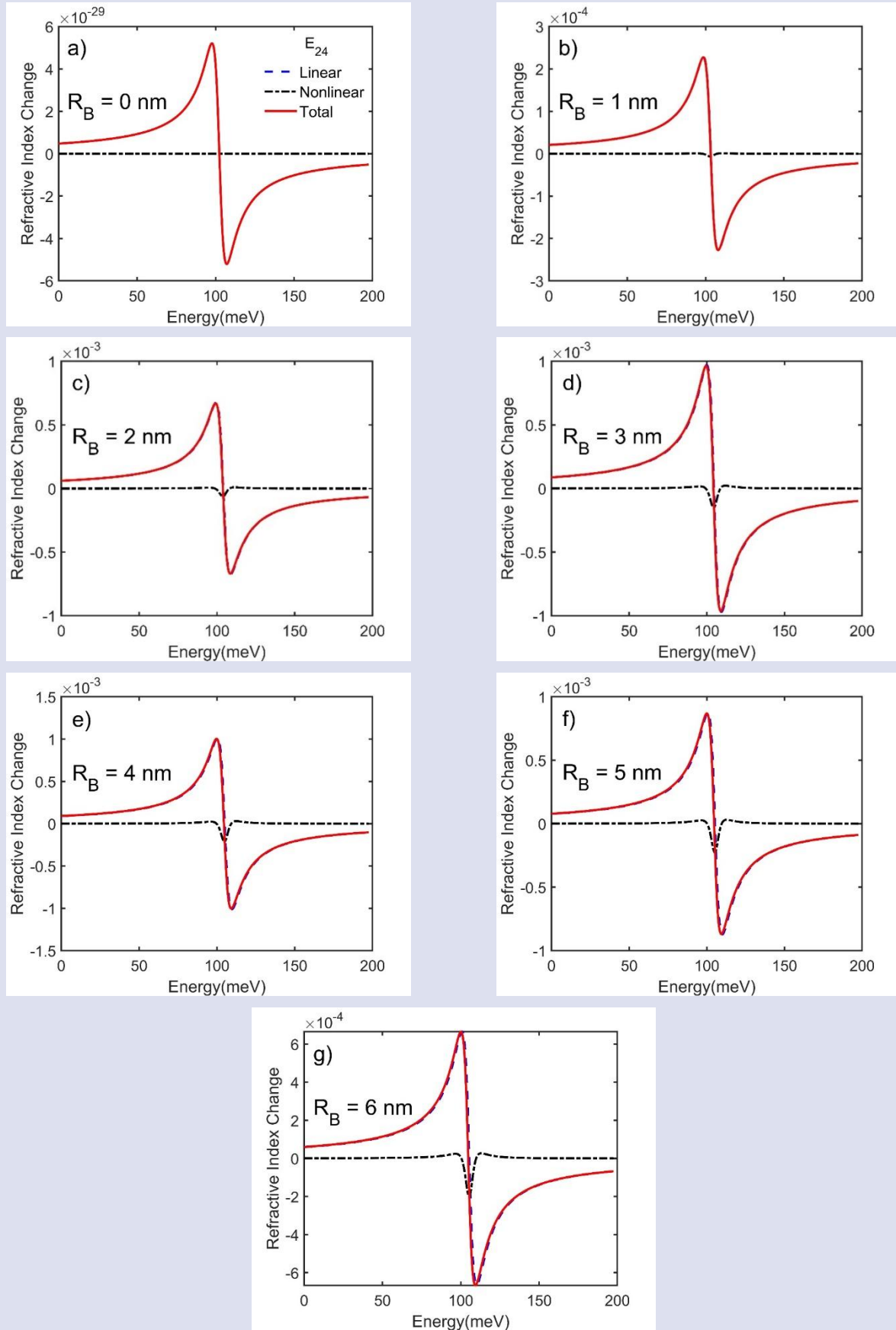


Figure 5. LRICs, NRICs and TRICs of the 2 – 4 transition for varying  $R_B$  thickness.

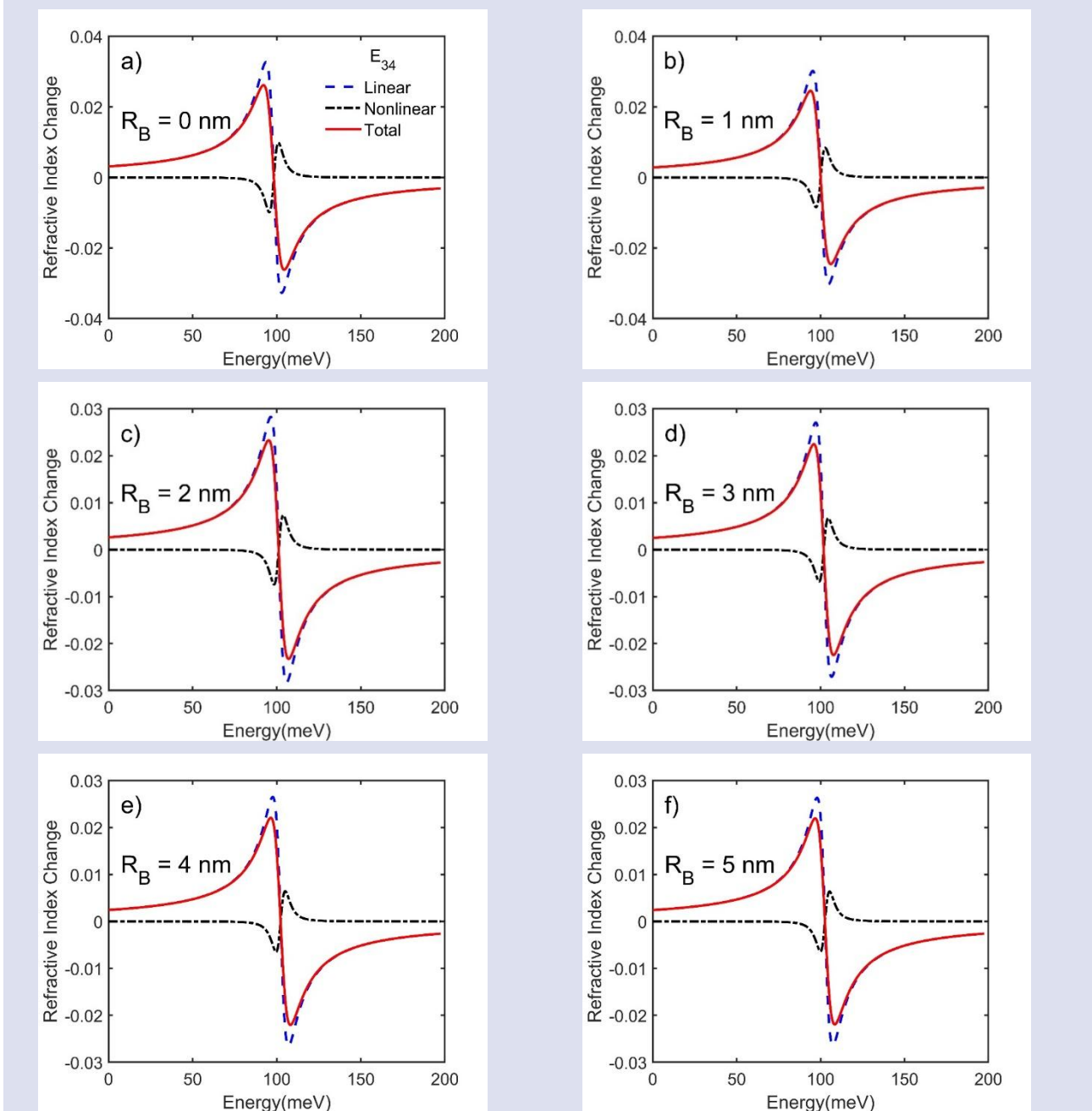
As shown in Figure 5, the refractive index change for the 2 – 4 transition is zero when the  $R_B$  is 0 nm, as expected. With an increase in  $R_B$  to 1 nm, very small

changes in the LRIC and NRIC are observed. Consequently, a slight variation in the TRIC is noted. Like the TAC, the TRIC reaches its maximum at an  $R_B$  thickness of 4 nm,

corresponding to the maximum point for  $M_{ij}$ . The variation in TRIC is around  $\pm 0.001$ , which is comparable to the values reported in the literature for other transitions [9-11]. While a blue shift is observed in the TRICs, it is negligible due to the steep variation in LRIC and NRIC.

The variation of the  $R_B$  affects LRICs and NRICs for the 3 – 4 transition in a linear and inverse linear manner, respectively, resulting in an almost constant TRIC, as shown in Figure 6. Consequently, the TRIC varies between

$\pm 0.006$  and  $\pm 0.009$  for  $R_B$  values ranging from 0 to 6 nm. This indicates that devices based on the 3 – 4 transition are only minimally affected by  $R_B$  variation, which could be advantageous for semiconductor device applications where thickness limitations are a concern. In addition, the 3 – 4 transition can be favored over the 2 – 4 transition due to its greater stability. The small energy differences between the 2 – 4 and 3 – 4 transitions make the 3 – 4 transition more suitable for terahertz (THz) device applications.



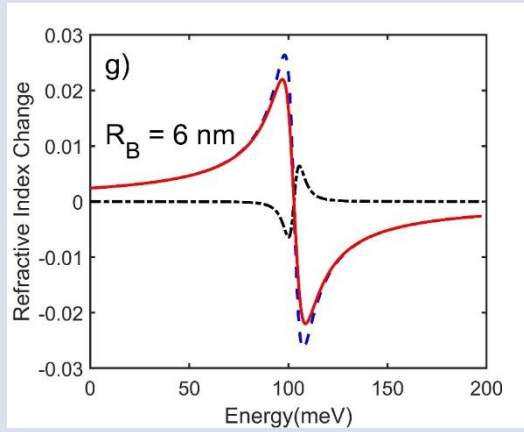


Figure 6. LRICs, NRICs and TRICs of the 3 – 4 transition for varying  $R_B$  thickness.

Table 1 presents the maximum values of the total AC and RIC for the 2 – 4 and 3 – 4 transitions. A similar trend is observed for both the AC and RIC coefficients. Breaking the symmetry through variations in the  $R_B$  thickness enhances the TAC of the 2 – 4 transitions, reaching its peak for an  $R_B$  thickness of 4 nm, while the TAC of the 3 –

4 transitions decreases. This indicates that 4 nm is the critical thickness for maximizing the TAC. Furthermore, the RIC coefficients are only slightly affected by these changes: the RIC of the 2 – 4 transitions increases, whereas the RIC of the 3 – 4 transitions decreases.

Table 1. Maximum values of the total AC and RIC of the 2-4 and 3-4 transitions.

RB (nm)	Total Maximum Values			
	TAC 2 – 4 ( $cm^{-1}$ )	TAC 3 – 4 ( $cm^{-1}$ )	RIC (2 – 4)	RIC (3 – 4)
0	0	1124	0	0.026
1	15	1119	0	0.024
2	45	1105	0	0.023
3	65	1101	0.001	0.022
4	69	1098	0.001	0.022
5	61	1090	0.001	0.022
6	48	1104	0.001	0.022

### Conclusion

In this study, the electronic and optical properties of a triple triangular QW structure based on GaAs/Al<sub>x</sub>Ga<sub>1-x</sub>As were analyzed with a focus on the 2 – 4 and 3 – 4 intersubband transitions. The influence of varying RB thicknesses (from 0 to 6 nm) on ELs, DMMEs, absorption coefficients, and refractive index changes were investigated. The results show that the RB thickness has a noticeable impact on the localization of WFs and symmetry of the potential. Specifically, increasing the RB thickness breaks the symmetry, leading to shifts in the energy levels and enabling the otherwise forbidden 2 – 4 transition. In contrast, the 3 – 4 transition remains more probable and consistent throughout the study, being only minimally affected by the RB variation. Quantitative analysis revealed that while both the 2 – 4 and 3 – 4 transitions exhibit slight energy shifts, the absorption coefficients of the 3 – 4 transition are significantly higher, supporting its greater transition probability. Notably, the TACs and TRICs of the 3 – 4 transition are relatively stable with respect to RB variation, unlike the 2 – 4 transition, which shows a peak in absorption at 4 nm RB before declining. This stability suggests that the 3 – 4 transition is more suitable for applications in semiconductor devices, especially where thickness limitations are critical.

Furthermore, the small energy difference between the 2 – 4 and 3 – 4 transitions makes the latter more viable for terahertz (THz) device applications. Overall, the 3 – 4 transition's robustness against structural variations and its high optical response make it a favorable candidate for high-performance THz devices, further supporting the significance of QW-based structures in next-generation semiconductor technologies.

### Conflict of Interest

There are no conflicts of interest in this work.

### Acknowledge

No acknowledgement

### Ethical Approval Statement

No ethical statement required

## References

- [1] Ozturk E., Sari H., Sokmen I., The dependence of the intersubband transitions in square and graded QWs on intense laser fields, *Solid State Communications*, 132(7) (2004) 497-502.
- [2] Sayrac H., Jaouane M., Ed-Dahmouny A., Sali A., Ungan F., Modulation of nonlinear optical rectification, second, and third harmonic generation coefficients in n-type quadruple  $\delta$ -doped GaAs quantum wells under external fields, *Physica B: Condensed Matter*, 690 (2024) 416252.
- [3] Restrepo R.L., Castaño-Vanegas L.F., Martínez-Orozco J.C., Morales A.L., Duque C.A., Mid-Infrared linear optical transitions in delta-doped AlGaAs/GaAs triple-quantum well, *Applied Physics A*, 125(1) (2018) 31.
- [4] Martínez-Orozco J.C., Mora-Ramos M.E., Duque C.A., The nonlinear optical absorption and corrections to the refractive index in a GaAs n-type delta-doped field effect transistor under hydrostatic pressure, *Physica Status Solidi B*, 249(1) (2012) 146-152.
- [5] Ozturk O., Alaydin B.O., Altun D., Ozturk E., Intense laser field effect on the nonlinear optical properties of triple quantum wells consisting of parabolic and inverse-parabolic quantum wells, *Laser Physics*, 32(3) (2022) 035404.
- [6] Alaydin B.Ö., Optical Properties of GaAs/Al<sub>x</sub>Ga<sub>1-x</sub>As Superlattice Under E-Field for Quantum Cascade Laser Application, *Gazi University Journal of Science*, 34(4) (2021) 1179-1191.
- [7] Dakhlaoui H., Linear and nonlinear optical absorption coefficients and refractive index changes in GaN/Al<sub>x</sub>Ga<sub>1-x</sub>N double quantum wells operating at 1.55  $\mu$ m, *Journal of Applied Physics*, 117(13) (2015).
- [8] Salman Durmuslar A., Investigation on nonlinear optical properties of symmetric and asymmetric double V-shaped Al<sub>x</sub>Ga<sub>1-x</sub>As/GaAs potential wells with structural parameters and external electromagnetic fields, *Philosophical Magazine*, 103(9) (2023) 872-891.
- [9] Rodríguez-Magdaleno K.A., Martínez-Orozco J.C., Rodríguez-Vargas I., Mora-Ramos M.E., Duque C.A., Asymmetric GaAs n-type double  $\delta$ -doped quantum wells as a source of intersubband-related nonlinear optical response: Effects of an applied electric field, *Journal of Luminescence*, 147 (2014) 77-84.
- [10] Barseghyan M.G., Hakimyfarid A., López S.Y., Duque C.A., Kirakosyan A.A., Simultaneous effects of hydrostatic pressure and temperature on donor binding energy and photoionization cross section in Pöschl–Teller quantum well, *Physica E: Low-dimensional Systems and Nanostructures*, 42(5) (2010) 1618-1622.
- [11] Karabulut İ., Atav Ü., Şafak H., Tomak M., Linear and nonlinear intersubband optical absorptions in an asymmetric rectangular quantum well, *The European Physical Journal B*, 55(3) (2007) 283-288.
- [12] Sayrac M., Effects of applied external fields on the nonlinear optical rectification, second, and third-harmonic generation in an asymmetrical semi exponential quantum well, *Optical and Quantum Electronics*, 54(1) (2021) 52.
- [13] Karimi M.J., Keshavarz A., Poostforush A., Linear and nonlinear intersubband optical absorption and refractive index changes of asymmetric double semi-parabolic quantum wells, *Superlattices and Microstructures*, 49(4) (2011) 441-452.
- [14] Niculescu E.C., Burileanu L.M., Radu A., Density of impurity states of shallow donors in a quantum well under intense laser field, *Superlattices and Microstructures*, 44(2) (2008) 173-182.
- [15] Liu G., Guo K., Zhang Z., Hassanbadi H., Lu L., Electric field effects on nonlinear optical rectification in symmetric coupled Al<sub>x</sub>Ga<sub>1-x</sub>As/GaAs quantum wells, *Thin Solid Films*, 662 (2018) 27-32.
- [16] Altun D., Ozturk O., Alaydin B.O., Ozturk E., Linear and nonlinear optical properties of a superlattice with periodically increased well width under electric and magnetic fields, *Micro and Nanostructures*, 166 (2022) 207225.
- [17] Nakamura K., Shimizu A., Koshiba M., Hayata K., Finite-element analysis of quantum wells of arbitrary semiconductors with arbitrary potential profiles, *IEEE Journal of Quantum Electronics*, 25(5) (1989) 889-895.
- [18] Karimi M.J., Keshavarz A., Second harmonic generation in asymmetric double semi-parabolic quantum wells: Effects of electric and magnetic fields, hydrostatic pressure and temperature, *Physica E: Low-dimensional Systems and Nanostructures*, 44(9) (2012) 1900-1904.
- [19] Ozturk E., Nonlinear optical absorption in graded quantum wells modulated by electric field and intense laser field, *The European Physical Journal B*, 75(2) (2010) 197-203.
- [20] Alaydin B.O., Altun D., Ozturk E., Linear and nonlinear optical properties of semi-elliptical InAs quantum dots: Effects of wetting layer thickness and electric field, *Thin Solid Films*, 755 (2022) 139322.
- [21] Kaynar E., Alaydin B.O., Optical properties of Al<sub>x</sub>In<sub>y</sub>Ga<sub>1-x-y</sub>As/Al<sub>z</sub>Ga<sub>w</sub>In<sub>1-z-w</sub>As quantum wells under electric and magnetic fields for telecommunication applications, *The European Physical Journal Plus*, 138(2) (2023) 121.
- [22] Alaydin B.O., Effect of high bandgap AlAs quantum barrier on electronic and optical properties of In<sub>0.70</sub>Ga<sub>0.30</sub>As/Al<sub>0.60</sub>In<sub>0.40</sub>As superlattice under applied electric field for laser and detector applications, *International Journal of Modern Physics B*, 35(02) (2021) 2150027.
- [23] Zhang Z.-H., Yuan J.-H., Guo K.-X., The Combined Influence of Hydrostatic Pressure and Temperature on Nonlinear Optical Properties of GaAs/Ga<sub>0.7</sub>Al<sub>0.3</sub>As Morse Quantum Well in the Presence of an Applied Magnetic Field, *Materials*, 11(5) (2018) 668.
- [24] Alaydin B.O., Altun D., Ozturk O., Ozturk E., High harmonic generations triggered by the intense laser field in GaAs/Al<sub>x</sub>Ga<sub>1-x</sub>As honeycomb quantum well wires, *Materials Today Physics*, 38 (2023) 101232.
- [25] Ozturk E., Nonlinear intersubband transitions in different shaped quantum wells under intense laser field, *Superlattices and Microstructures*, 82 (2015) 303-312.